



*Supplement of*

**Photolytically induced changes in composition and volatility of biogenic secondary organic aerosol from nitrate radical oxidation during night-to-day transition**

**Cheng Wu et al.**

*Correspondence to:* David M. Bell ([david.bell@psi.ch](mailto:david.bell@psi.ch)) and Claudia Mohr ([claudia.mohr@aces.su.se](mailto:claudia.mohr@aces.su.se))

The copyright of individual parts of the supplement might differ from the article licence.

## Supporting information

### S1 Data analysis of FIGAERO-CIMS

Data from the FIGAERO-CIMS was analysed with Tofware (Aerodyne Research, Inc. and Tofwerk AG) and Igor Pro (WaveMetrics Inc.). The initial mass calibration was conducted on  $\text{I}^+$ ,  $\text{IH}_2\text{O}^+$ ,  $\text{IHNO}_3^+$ , and  $\text{I}_3^+$ . In addition, the chemical composition of the 2–3 major dimer peaks were confirmed by the compounds measured simultaneously by the EESI-TOF, and these clearly identified ions were used as mass calibrants as well for the mass range higher than 400 Th. After processing the high resolution (HR) ion fits, the subsequent treatment of the processed HR data was performed using code written with MATLAB for checking signal to noise ratio, integrating thermogram data, etc.

#### S1.1 Background subtraction

For each experiment, one particle blank (zero sampling time + normal heating) was performed during dark aging. Because the background signal varies for each filters/experiment, when subtracting the background from the signals of normal filters, the integrated area of the particle blank from the same experiment was scaled up/down with a scaling factor. This factor was determined by comparing the detected signals of the last 1min of “temp soak” of the normal heating to the detected signals of the last 1min of “temp soak” of the zero heating) (Fig. S1).

#### S1.2 Impact of thermal decomposition on FIGAERO particle phase measurement

For the FIGAERO inlet, the artefacts associated with thermal decomposition have been discussed in many previous studies (Lopez-Hilfiker et al., 2015; D'Ambro et al., 2019; Stark et al., 2017). We corrected the impact of thermal decomposition for further analysis on the chemical composition and temperature at maximum desorption rate ( $T_{\text{max}}$ ) with the following steps:

- (1) If the thermogram of a compound exhibited multiple peaks (Fig. S2a),  $T_{\text{max}}$  was determined based on the first peak, and the peak area was integrated only for the first peak.
- (2) If the thermogram of a compound was monomodal, but  $T_{\text{max}}$  was “too high” based on its chemical composition (e.g.,  $\text{C}_5\text{H}_{10}\text{N}_2\text{O}_9$  has a similar  $T_{\text{max}}$  as that of  $\text{C}_{10}\text{H}_{17}\text{N}_3\text{O}_{13}$ , Fig. S2b), this compound was excluded from the analysis of the chemical composition.

Fig. S3 shows thermal fragmentation to be a minor issue in our study. Most of the peaks in the three systems do not have “shoulders” or “plateaus”. In addition, for almost all compounds in the isoprene and  $\alpha$ -pinene systems and the monomers in the  $\beta$ -caryophyllene system, the signals in the temperature range higher than 120 °C where dehydration or decarboxylation reactions are expected to occur

(Buchholz et al., 2020; Stark et al., 2017) are relatively low. There are a few exceptions with bi-modal thermograms (Fig. S3c, blue lines), which were corrected for as described above. Regarding the dimers from the  $\beta$ -caryophyllene system (Figure S3d), there are a few compounds with significant tailings. However, their molecular formulae do not correspond to thermal decomposition products of major dimers (e.g. dehydration products with  $m/z - 18.015$  compared to the parent compounds), but the tailings might rather be signal from isomers of these major dimers.

### **S1.3 Uncertainties in the gas-phase measurement**

The uncertainties in the gas-phase measurement due to the changing ratios of  $I^-/NO_3^-$  were tested after Exp. 2 (isoprene +  $NO_3$ ). The total gas phase flow for the FIGAERO-CIMS was  $5\text{ L min}^{-1}$  and it was partly replaced by 1.5, 3.0, 4.0  $\text{L min}^{-1}$   $N_2$  with keeping the total flow constant, causing  $I^-/NO_3^- = 0.09$  (no dilution), 0.14, 0.28 and 1.6. In Fig. S4, three major gas-phase compounds  $C_5H_{10}IN_2O_8^-$ ,  $C_5H_9INO_6^-$ ,  $C_5H_9IN_3O_{10}^-$  were chosen and their normalized signals (to the signals measured without dilution and with the consideration of dilution rates) were compared. The normalized signal didn't change significantly with decreasing  $I^-/NO_3^-$  as long as  $I^-/NO_3^-$  was higher than  $\sim 0.3$ , but it decreased about 20–40% when  $I^-/NO_3^-$  decreased further and was close to 0.1.

### **S2 Size dependence of light absorption**

In Fig. S5, we simulated the difference between the mass absorption efficiency ( $m^2\text{ g}^{-1}$ , MAE) at wavelength = 350 nm of larger particles (diameter = 300 nm) versus smaller particles (diameter = 100 nm) as a function of an imaginary part of the refractive index using MiePlot, based on the equations found elsewhere (Bohren and Huffman, 1998). The imaginary part of the refractive index corresponds to species that absorb light. With a value of 0.001, the MAE of 300 nm particles is 1.7 times higher than the MAE of 100 nm particles. Although no direct measurement of the imaginary part of the refractive index was conducted in this study, based on a summary of different SOA systems by (Nakayama et al., 2015) and the study of He et al. (2021), a value between 0.001 and 0.01 could be expected for biogenic VOC species studied here.

## SI Figures

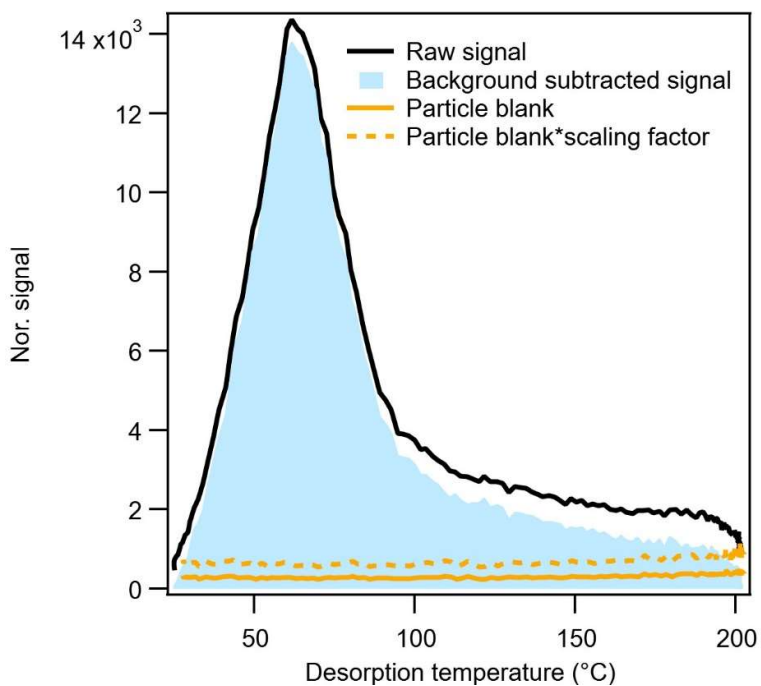


**Fig. S1 Thermogram background subtraction for a typical compound  $C_{10}H_{16}N_2O_{10}$  from Exp.2: isoprene +  $NO_3$ .**

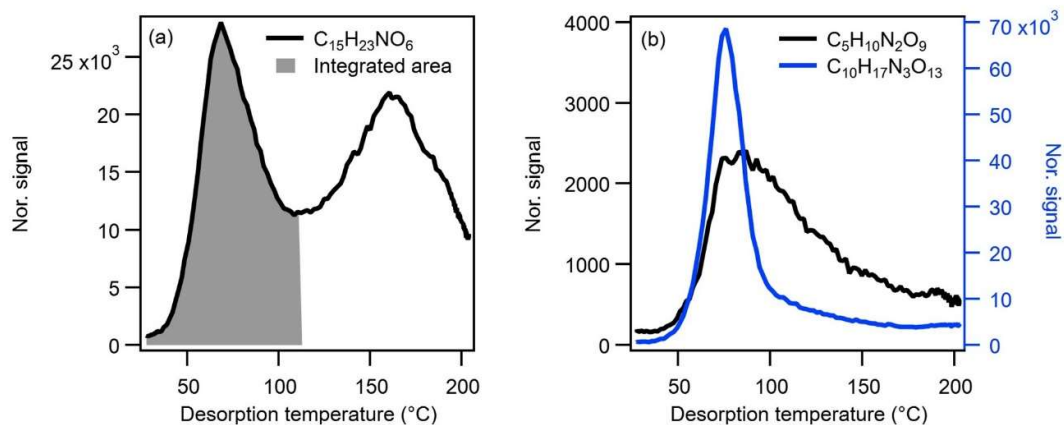


**Fig. S2 (a) Thermogram of  $C_{15}H_{23}NO_6$ , the shaded area represents the integrated area. (b) Thermogram of  $C_5H_{10}N_2O_9$ , compared to that of  $C_{10}H_{17}N_3O_{13}$  from a filter sample of Exp. 1: isoprene +  $NO_3$ .**

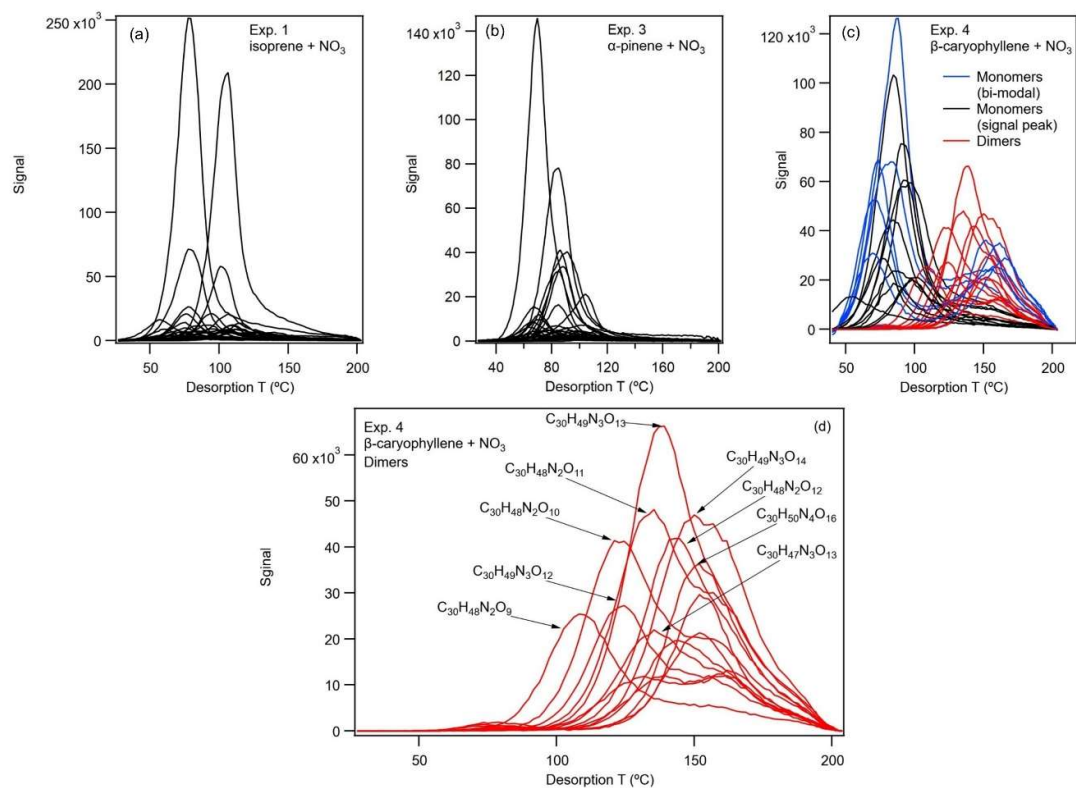


**Fig. S3 Thermograms of top 30 (signal) compounds of the SOA from (a) Exp.1, (b) Exp. 3 and (c) Exp. 4 and (d) major dimers from Exp. 4.**

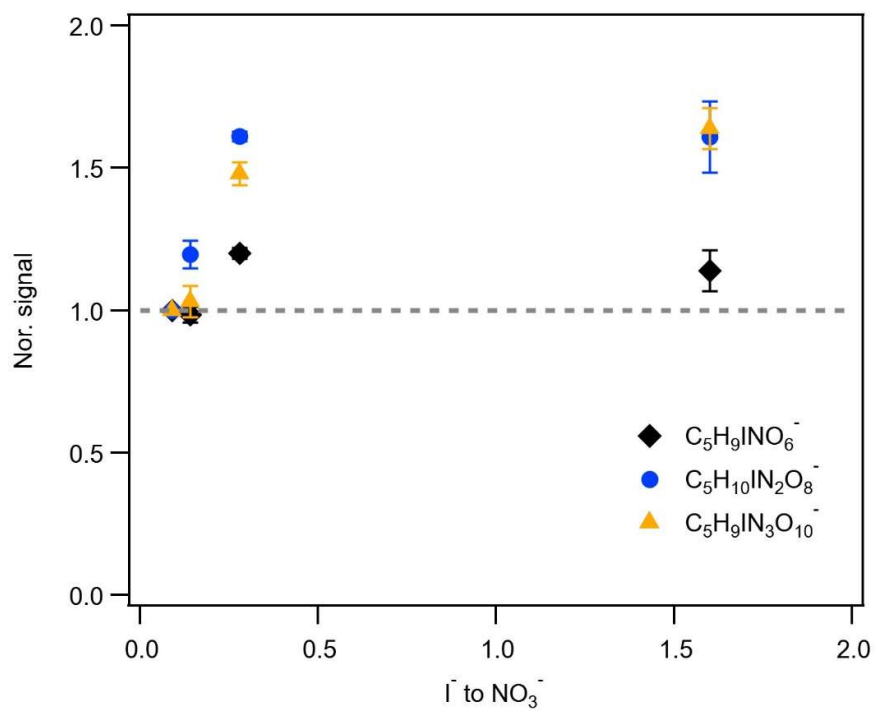


**Fig. S4 Normalized signal of three major compounds in the gas phase from Exp. 2: isoprene +  $NO_3$  as a function of  $I^-/NO_3^-$  ratio.**

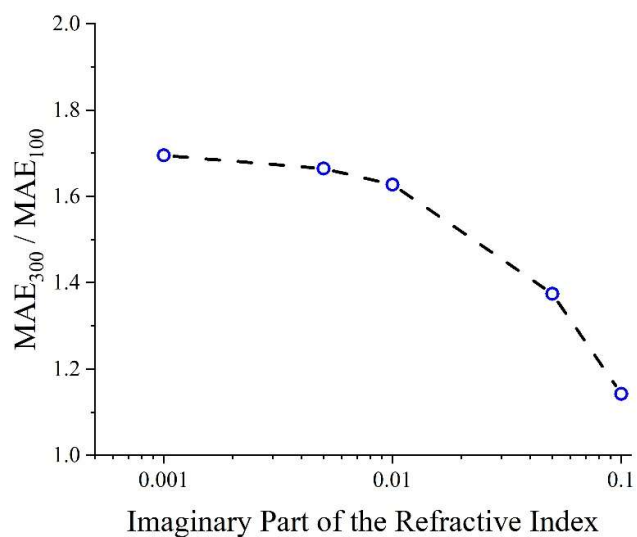


**Fig. S5 Mass absorption efficiency (MAE) of 300 nm particles versus that of 100 nm particles at wavelength of 300 nm, as a function of imaginary part of the refractive index.**

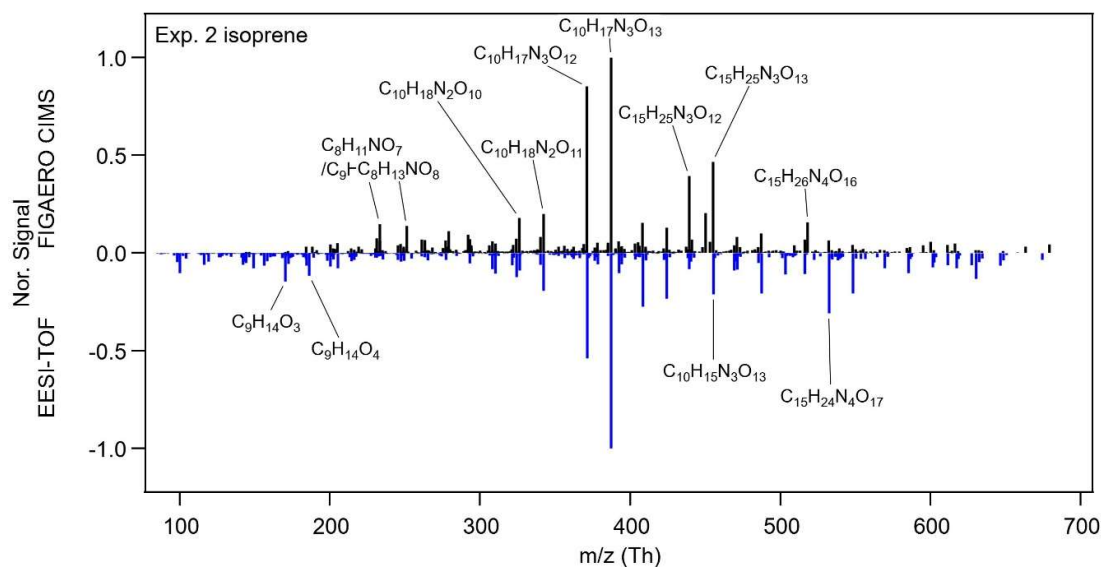


**Fig. S6** FIGAERO-CIMS (positive axis) and EESI-TOF (negative axis) mass spectra of particle phase  $C_xH_yO_zN_{0-4}$  formed during Exp. 2: isoprene +  $NO_3$  shortly before photolysis. For the FIGAERO-CIMS, the last filter before photolysis is chosen. The EESI-TOF mass spectra are averaged mass spectra during the same sampling time as that of FIGAERO-CIMS. All mass spectra are normalized to the corresponding maximal signal.

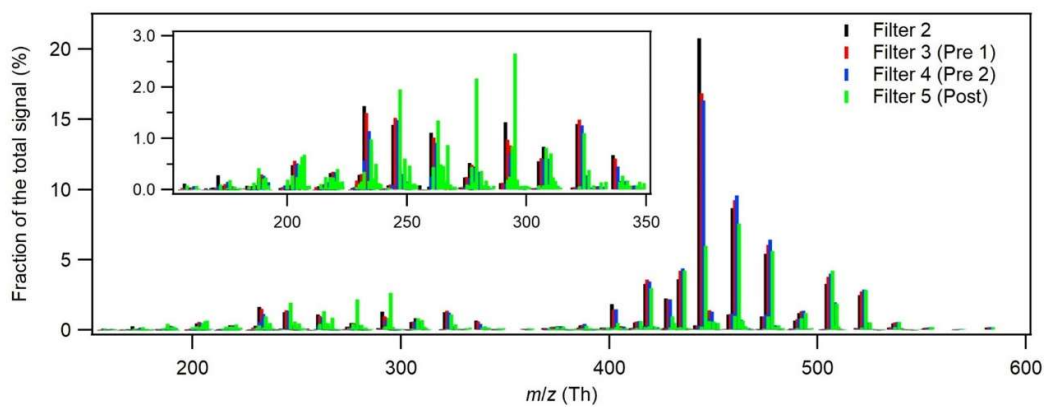


**Fig. S7** Mass spectra of four filter collected during dark aging and photolysis in Exp. 3.

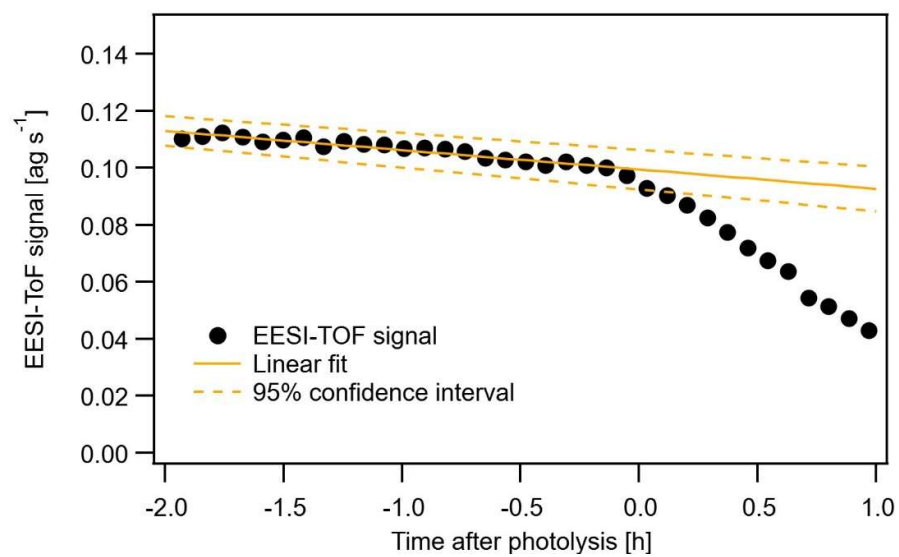


**Fig. S8** Time series of  $\text{C}_{10}\text{H}_{17}\text{N}_3\text{O}_{13}$  measured by the EESI-TOF and linear fit (with 95% confidence interval) of the 2 h pre-photolysis data points.



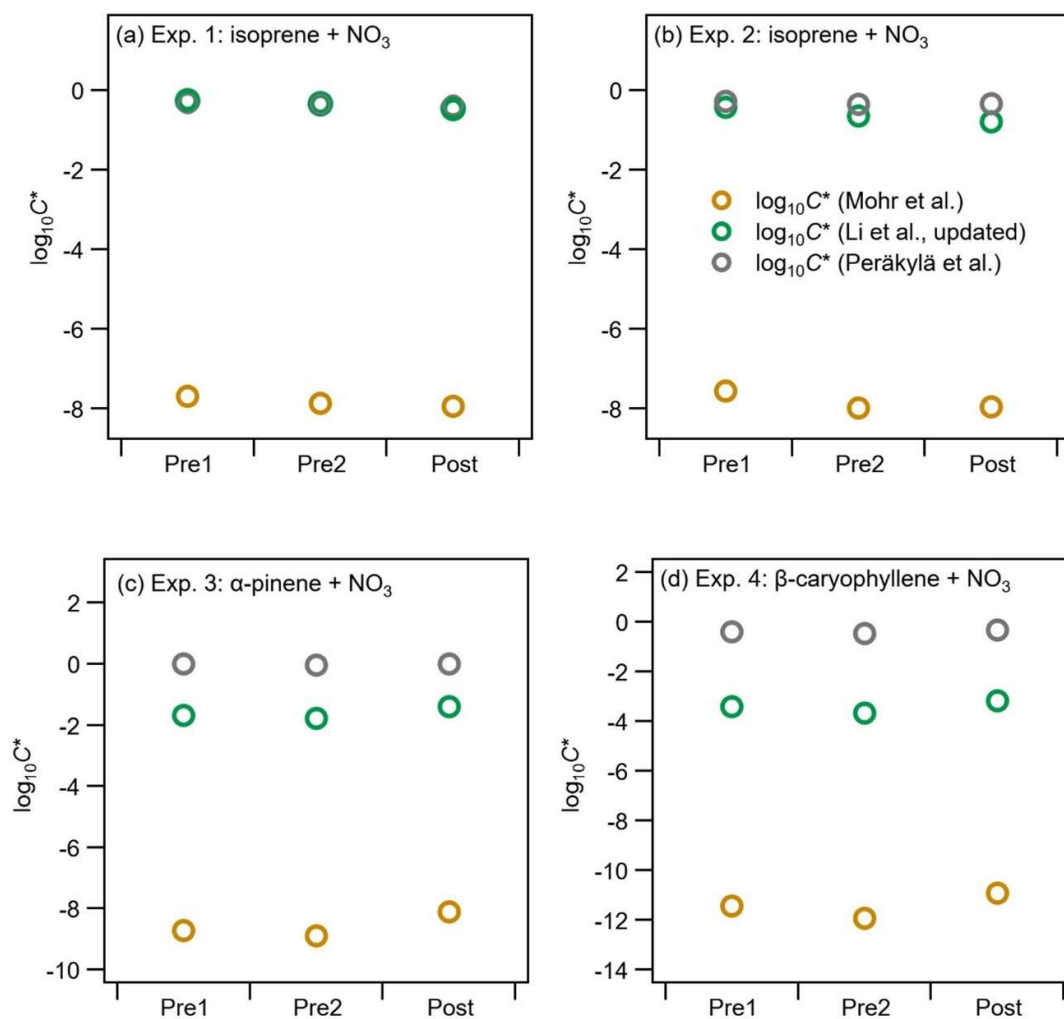


**Fig. S9 Bulk  $\log_{10}C^*$  calculated by Mohr et al. (2019), Li et al. (2016) (updated by Isaacman-VanWertz and Aumont (2021)), Peräkylä et al. (2020) for the three filters (Pre 1, Pre 2 and Post) from all experiments.**

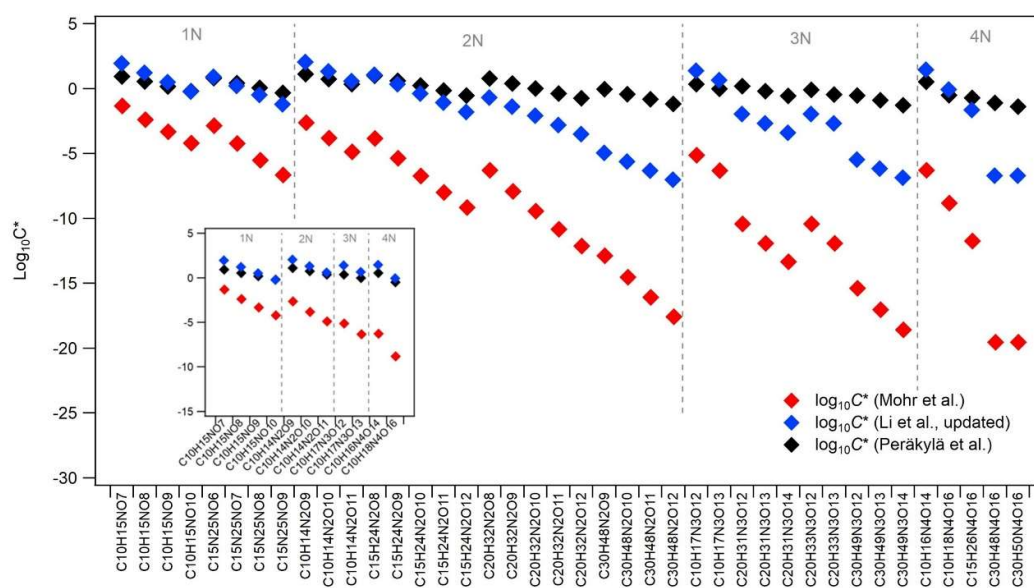


**Fig. S10  $\log_{10}C^*$  based on the parameterizations of Mohr et al. (2019), Li et al. (2016) (updated by Isaacman-VanWertz and Aumont (2021)), and Peräkylä et al. (2020) of major compounds with 1 – 4 N from all three systems. In the small panel, only C10 compounds are compared.**

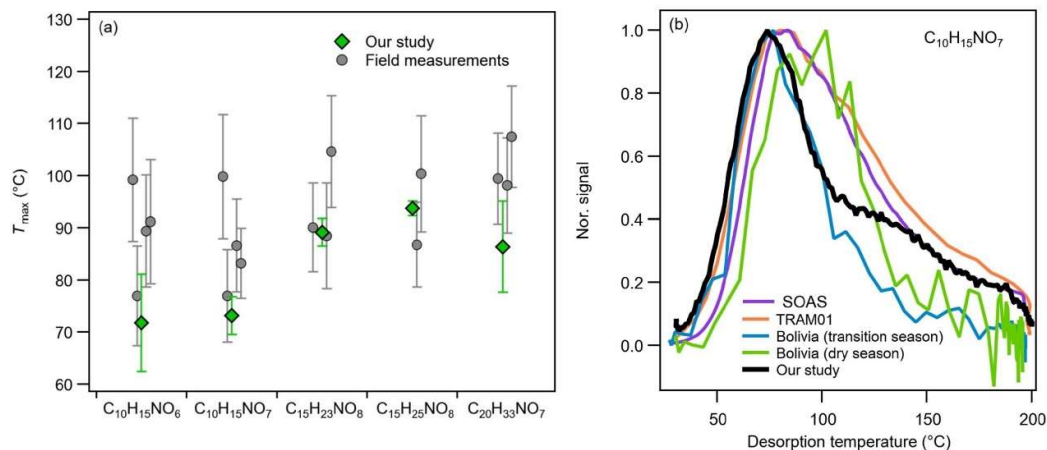


**Fig. S11 (a) Comparison between the average  $T_{\max}$  with standard deviation of  $C_{10}H_{15}NO_{6,7}$ ,  $C_{15}H_{23,25}NO_8$  and  $C_{20}H_{33}NO_7$  from our study (mass loadings between  $\sim 0.3$  and  $\sim 3 \mu\text{g}$ ) including both dark aging and photolysis periods and three field campaigns: SOAS (Lopez-Hilfiker et al., 2016), TRAM01 (Huang et al., 2019) and the Bolivia campaign (during both transition season and dry season, Huang et al. in preparation). (b) Average thermograms of  $C_{10}H_{15}NO_7$  from our study and the field campaigns. The mean mass loading was  $0.33 \pm 0.22$ ,  $1.45 \pm 0.95$ ,  $0.07 \pm 0.06$  and  $0.21 \pm 0.16 \mu\text{g}$ , and the time of ramping the temperature of the nitrogen flow from ambient temperature up to  $200^\circ\text{C}$  was 20, 15, 15 and 15 min for SOAS, TRAM01, Bolivia (transition season) and Bolivia (dry season), respectively.**

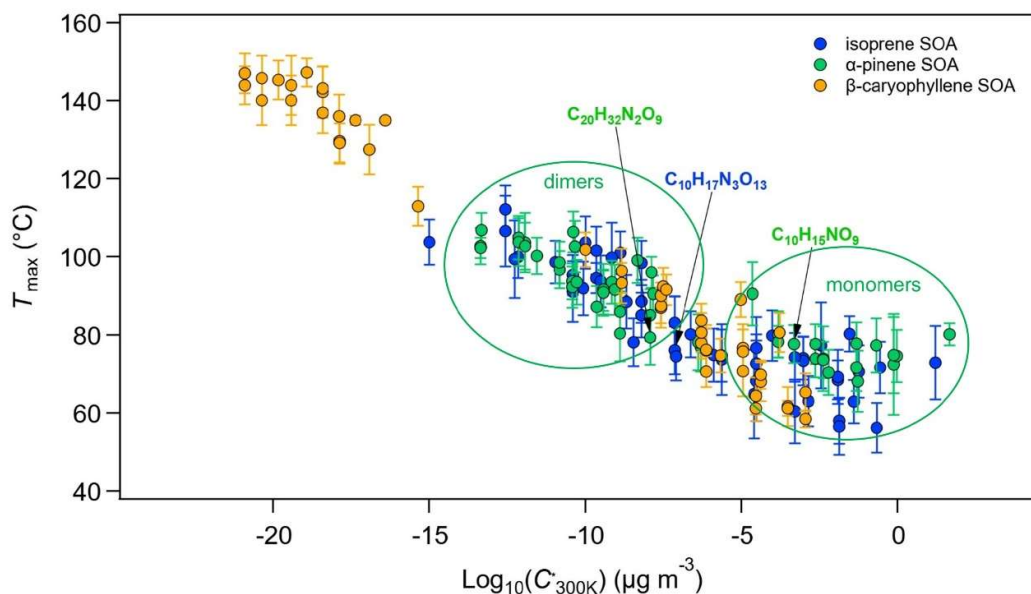


**Fig. S12** Average  $T_{\max}$  from all filter samples during dark aging and photolysis versus saturation concentration  $\log_{10}C^*$  by Mohr et al. (2019) of top 50 compounds from the isoprene,  $\alpha$ -pinene SOA and  $\beta$ -caryophyllene SOA. Green circles indicating regions dominated by the monomers and dimers of  $\alpha$ -pinene SOA are added to guide the eye.

## SI References

- Bohren, C. F., and Huffman, D. R.: Appendix a: Homogeneous sphere, Absorption and scattering of light by small particles, Wiley-VCH Verlag GmbH, 477482, 1998.
- Buchholz, A., Ylisirniö, A., Huang, W., Mohr, C., Canagaratna, M., Worsnop, D. R., Schobesberger, S., and Virtanen, A.: Deconvolution of FIGAERO-CIMS thermal desorption profiles using positive matrix factorisation to identify chemical and physical processes during particle evaporation, *Atmos. Chem. Phys.*, 20, 7693-7716, 10.5194/acp-20-7693-2020, 2020.
- D'Ambro, E. L., Schobesberger, S., Gaston, C. J., Lopez-Hilfiker, F. D., Lee, B. H., Liu, J., Zelenyuk, A., Bell, D., Cappa, C. D., Helgestad, T., Li, Z., Guenther, A., Wang, J., Wise, M., Caylor, R., Surratt, J. D., Riedel, T., Hyttinen, N., Salo, V. T., Hasan, G., Kurtén, T., Shilling, J. E., and Thornton, J. A.: Chamber-based insights into the factors controlling epoxydiol (IEPOX) secondary organic aerosol (SOA) yield, composition, and volatility, *Atmos. Chem. Phys.*, 19, 11253-11265, 10.5194/acp-19-11253-2019, 2019.
- He, Q., Tomaz, S., Li, C., Zhu, M., Meidan, D., Riva, M., Laskin, A., Brown, S. S., George, C., Wang, X., and Rudich, Y.: Optical Properties of Secondary Organic Aerosol Produced by Nitrate Radical Oxidation of Biogenic Volatile Organic Compounds, *Environmental Science & Technology*, 55, 2878-2889, 10.1021/acs.est.0c06838, 2021.
- Huang, W., Saathoff, H., Shen, X., Ramisetty, R., Leisner, T., and Mohr, C.: Chemical Characterization of Highly Functionalized Organonitrates Contributing to Night-Time Organic

- Aerosol Mass Loadings and Particle Growth, *Environ Sci Technol*, 53, 1165-1174, 10.1021/acs.est.8b05826, 2019.
- Isaacman-VanWertz, G., and Aumont, B.: Impact of organic molecular structure on the estimation of atmospherically relevant physicochemical parameters, *Atmos. Chem. Phys.*, 21, 6541-6563, 10.5194/acp-21-6541-2021, 2021.
- Li, Y., Pöschl, U., and Shiraiwa, M.: Molecular corridors and parameterizations of volatility in the chemical evolution of organic aerosols, *Atmos. Chem. Phys.*, 16, 3327-3344, 10.5194/acp-16-3327-2016, 2016.
- Lopez-Hilfiker, F. D., Mohr, C., Ehn, M., Rubach, F., Kleist, E., Wildt, J., Mentel, T. F., Carrasquillo, A. J., Daumit, K. E., Hunter, J. F., Kroll, J. H., Worsnop, D. R., and Thornton, J. A.: Phase partitioning and volatility of secondary organic aerosol components formed from  $\alpha$ -pinene ozonolysis and OH oxidation: the importance of accretion products and other low volatility compounds, *Atmos. Chem. Phys.*, 15, 7765-7776, 10.5194/acp-15-7765-2015, 2015.
- Lopez-Hilfiker, F. D., Mohr, C., D'Ambro, E. L., Lutz, A., Riedel, T. P., Gaston, C. J., Iyer, S., Zhang, Z., Gold, A., Surratt, J. D., Lee, B. H., Kurten, T., Hu, W. W., Jimenez, J., Hallquist, M., and Thornton, J. A.: Molecular Composition and Volatility of Organic Aerosol in the Southeastern U.S.: Implications for IEPOX Derived SOA, *Environmental Science & Technology*, 50, 2200-2209, 10.1021/acs.est.5b04769, 2016.
- Mohr, C., Thornton, J. A., Heitto, A., Lopez-Hilfiker, F. D., Lutz, A., Riipinen, I., Hong, J., Donahue, N. M., Hallquist, M., Petäjä, T., Kulmala, M., and Yli-Juuti, T.: Molecular identification of organic vapors driving atmospheric nanoparticle growth, *Nature Communications*, 10, 4442, 10.1038/s41467-019-12473-2, 2019.
- Nakayama, T., Sato, K., Tsuge, M., Imamura, T., and Matsumi, Y.: Complex refractive index of secondary organic aerosol generated from isoprene/NO<sub>x</sub> photooxidation in the presence and absence of SO<sub>2</sub>, *Journal of Geophysical Research: Atmospheres*, 120, 7777-7787, <https://doi.org/10.1002/2015JD023522>, 2015.
- Peräkylä, O., Riva, M., Heikkinen, L., Quéléver, L., Roldin, P., and Ehn, M.: Experimental investigation into the volatilities of highly oxygenated organic molecules (HOMs), *Atmos. Chem. Phys.*, 20, 649-669, 10.5194/acp-20-649-2020, 2020.
- Stark, H., Yatavelli, R. L. N., Thompson, S. L., Kang, H., Krechmer, J. E., Kimmel, J. R., Palm, B. B., Hu, W., Hayes, P. L., Day, D. A., Campuzano-Jost, P., Canagaratna, M. R., Jayne, J. T., Worsnop, D. R., and Jimenez, J. L.: Impact of Thermal Decomposition on Thermal Desorption Instruments: Advantage of Thermogram Analysis for Quantifying Volatility Distributions of Organic Species, *Environmental Science & Technology*, 51, 8491-8500, 10.1021/acs.est.7b00160, 2017.